Summary of Research (Final Report)
for the period 1 July 1994 - 30 November 1996*

for

NASA-Ames Grant No. NAG 2-938

entitled

ADAPTATION OF AN IN SITU GROUND-BASED TROPOSPHERIC OH/HO2 INSTRUMENT FOR AIRCRAFT USE

submitted to

Ms. Barbara Hastings
Administrative Grants Officer
NASA-Ames Research Center
Moffett Field CA 94035-1000

by

William H. Brune
Principal Investigator
Department of Meteorology

The Pennsylvania State University
Office of Sponsored Programs
110 Technology Center
University Park PA 16802

April 2, 1997

*performance period includes 90-day pre-award and 60-day no-cost extension

Introduction.

In-situ HO_x (OH and HO_2) measurements are an essential part of understanding the photochemistry of aircraft exhaust in the atmosphere. HO_x affects the partitioning of nitrogen species in the NO_y family. Its reactions are important sources and sinks for tropospheric ozone, thus providing a link between the NO_x in aircraft exhaust and tropospheric ozone. OH mixing ratios are enhanced in aircraft wakes due to the photolysis of the HONO that is made close to the engine. Measurements of HO_x in aircraft wakes, along with NO_x measurements, thus provides a constraint on chemical models of the engine combustion and exhaust.

NASA-Ames Grant No. NAG 2-938, "Adaption of an in situ ground-based tropospheric OH/HO_2 instrument for aircraft use" supported our development of the Airborne Tropospheric Hydrogen Oxides Sensor (ATHOS). Within the two years of this grant, we designed, developed, and successfully flew this instrument. It was part of the instrument complement on board the NASA DC-8 during SUCCESS, which took place in Kansas in April and May, 1996. ATHOS has a limit-of-detection for OH (S/N=2) of 10^5 OH molecules cm^{-3} in less than 150 seconds. While this sensitivity is about 2-3 times less than the initial projections in the proposal, it is more than adequate for good measurements of OH and HO_2 from the planetary boundary layer to the stratosphere. Our participation in SUCCESS was to be engineering test flights for ATHOS; however, the high-quality measurements we obtained are being used to study HO_x photochemistry in contrails, clouds, and the clear air.

The ATHOS Instrument.

ATHOS uses laser induced fluorescence to measure OH and HO_2 simultaneously (Stevens et al., 1994; Brune et al., 1995; Mather et al., 1997). OH is both excited and detected with an $A^2\Sigma^+$ (v'=0) $\rightarrow$ $X^2\Pi$ (v"=0) transition near 308 nm. Because OH is excited and detected at the same wavelength, the weak OH fluorescence signal must be separated from the much stronger Rayleigh and wall scattering signals. At low pressure, the OH fluorescence decays much more slowly than the background scattering. Thus, by pulling the air sample into a low pressure detection chamber and gating the detector on only after the background scattering has ceased, the OH fluorescence can be detected above only a small background signal (Hard and O'Brien, 1984; Hard et al., 1992; Hard et al., 1995; O'Brien and Hard, 1993).

HO_2 is detected by adding to the low pressure flow NO, which reacts with HO_2 to form OH. The resultant OH is then detected with laser induced fluorescence. OH and HO_2 can be measured simultaneously by having two detection axes and adding the NO in front of the second one.

Front and side views of the ATHOS instrument are shown in Figure 1. ATHOS is mounted in the forward cargo bay of the DC-8, roughly at station 430 (11 m from the nose). It comes in three pieces: the detection system, the electronics system, and the

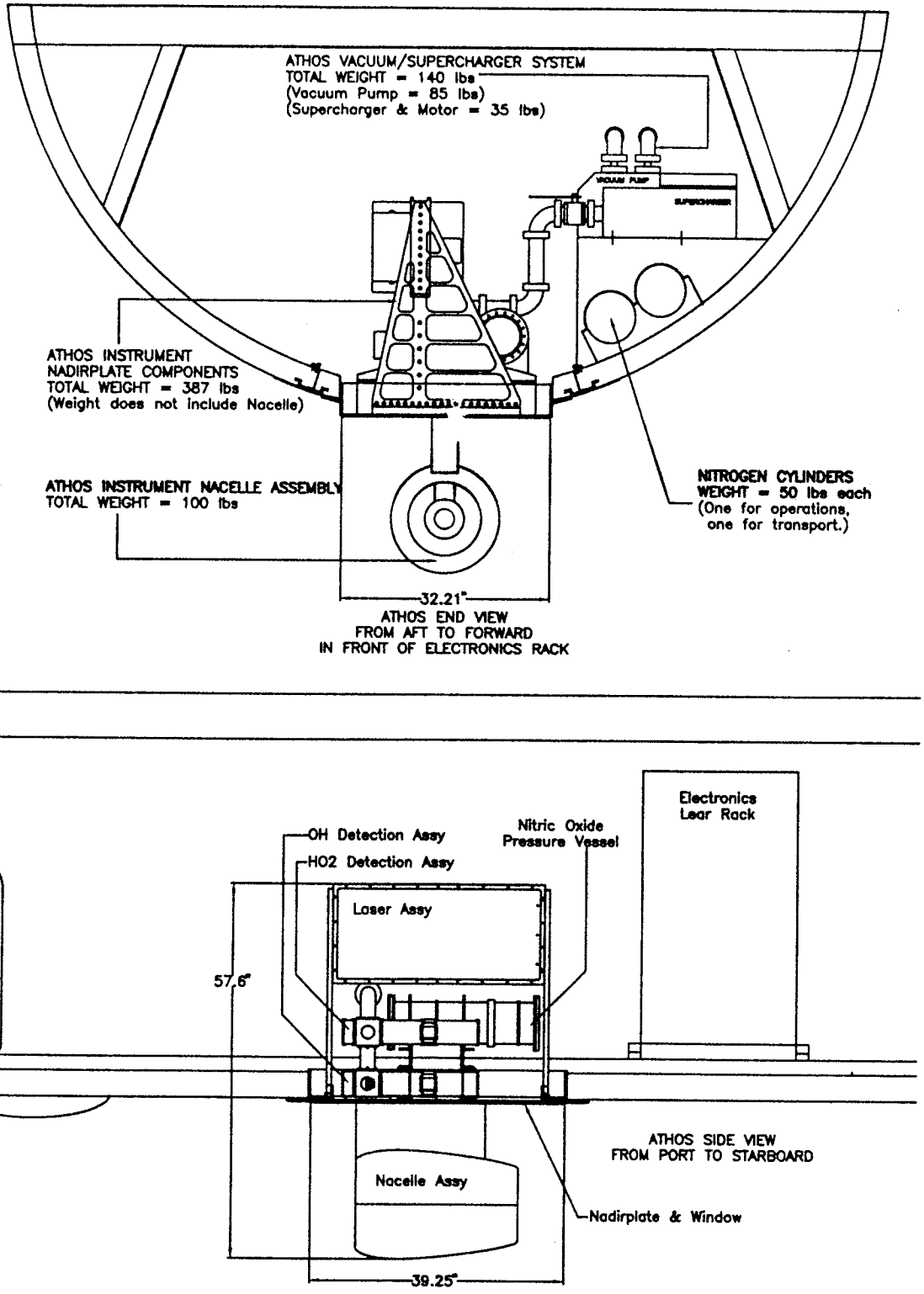

Figure 1. Drawings of ATHOS in the forward cargo bay. The top drawing is looking aft; the bottom looking from port to starboard. The sampling inlet (not shown) is 2 cm off of the top inner surface of the inner nacelle.

vacuum pumping system. The detection system sits on a plate that fits into the new nadir #2 hatch. Its characteristics are given in Table 1.

Table 1. ATHOS Weight, Volume, and Electrical Power Consumption

Forward Cargo Bay	**Weight (kg)**	**Inside Volume (m^3)**
detection assembly	175	0.6
nacelle assembly	45	0.0
vacuum pumps	65	0.3
electronics rack	130	0.4
Main Cabin	15	1/2 Rack, 2 seats
Total	**430**	**1.3**
Electrical Power (VA)	60 Hz, 1 phase	400 Hz, 3 phase
	2400	**1550**
Total (VA)		**4150**

Being in the forward cargo bay has several advantages. First, the inlet is near the front of the aircraft where the aircraft boundary layer is smaller. Second, the sampling nacelle does not interfere with sampling inlets from other instruments downstream. Third, more valuable floor space is gained in the main cabin at the expense of a small amount of space in the forward cargo pit. Being in the cargo bay has a few disadvantages. First, the temperature in the cargo bays is not as well controlled as in the main cabin, and thus better instrument thermal control is important. Second, runway debris thrown up by the wheel on the front landing gear might cause instrument damage, although none occurred during SUCCESS. Overall, the advantages outweigh the disadvantages.

The operation of ATHOS is similar to the earlier ground-based instrument described in Stevens et al. (1994) and the Harvard HOx instrument on the ER-2 described by Wennberg et al. (1994, 1995). Please refer to Stevens et al. (1994) and Aschmutat et al., (1995) for more detailed descriptions of the instrument calibration. A brief description of the ATHOS operation follows.

The ambient air is slowed from aircraft speed of roughly 250 m s^{-1} to a range of velocities between 7 and 40 m s^{-1} in an aerodynamic nacelle assembly, consisting of two nested nacelles designed by Kevin James at NASA Ames. These nacelles are set 18 cm away from the fuselage to avoid sampling the aircraft boundary layer, which is about 14 cm at the nacelles. A pitot tube measures the air velocity in the nacelle and an array of thermistors across the inner nacelle indicates intrusion of warm, boundary layer air into air sampled by the instrument inlet. The velocity of the air at the sampling inlet is controlled by a centerbody (not shown) that moves closer or away from the rear of the inner nacelle.

The slowed air is then pulled at right angles through a 0.056" diameter inlet, up a 39-cm long, 5-cm diameter tube, into low-pressure detection chambers by a vacuum pump (Eaton M45 Supercharger backed by a Leybold D25B vacuum pump - 32 L s^{-1} pumping speed) and is exhausted at the rear of the aircraft. The pressure in the detection cells

ranges from 4 to 12 mb, depending on the altitude, and the temperature in the detection axes is typically at 260 to 280 K.

Detection occurs in the detection chambers at the intersections of the airflow, the laser beams that are passed through multipass White cells, and the detector fields-of-view. The first detection cell encountered by the air stream is for OH. The second cell for HO_2 is 10 cm downstream of the first. A Teflon loop positioned between the axes is used to add reagent NO for converting HO_2 to OH. Because of the two-axis arrangement, the detection of OH and HO_2 is truly simultaneous.

The laser is a combination of a Lightwave 210G diode-pumped frequency-doubled Nd:YAG laser (532 nm; 5 kHz repetition rate, 35 ns long pulses) which pumps a Harvard-designed frequency-doubled dye laser, based on a Chromatix design (Wennberg et al., 1994). This dye laser has an intracavity etalon that both narrows the laser linewidth to 3.5 GHz, about the OH linewidth, and allows for tuning on and off the OH resonance. The laser is tuned on and off resonance with the OH transition (called on-line and off-line) every 10 seconds to determine OH fluorescence and background signals. The OH transition usually used is either the $P_1(1)$ or the $Q_1(2)$ near 308 nm. The UV laser power was typically 8 -15 mW.

Collection optics gather about 8% of the fluorescence and send it to detectors behind narrow-band 308 nm interference filters. The detectors (Hamamatsu gated microchannel plate detectors) are gated on for 300 ns to detect the OH fluorescence 40 ns after each laser pulse has cleared the detection cells. Two counter gates are used for each detector: one counts the OH fluorescence signal; a second counts the Rayleigh and chamber scattering for 50 ns during the laser pulse when the detector gate is off and the detector gain is 1000 times less. A small amount of the light going to the OH microchannel plate detector is picked off and sent through a 332 nm interference filter to a photomultiplier detector in order to monitor the N_2 Raman scattering.

A reference cell containing OH made on a hot filament indicates when the laser is on-line and off-line with the OH transition (Stevens et al., 1994; Wennberg et al., 1994). The off-line position alternates between a longer and a shorter wavelength than the on-line position to test the flatness of the background signal. A spectral scan is taken every hour to identify the laser line and to measure the background signal shape. An on-line stepping routine continually tests for the largest reference cell signal and adjusts the on-line position accordingly.

HO_2 is detected by adding NO inside the flow tube leading to the second detection chamber. The reaction of NO with HO_2 produces OH, which is detected by laser induced fluorescence. The NO flow rate is occasionally varied to insure that maximum conversion of HO_2 to OH is occurring.

An in-flight calibration system creates OH and HO_2 in equal amounts outside the detection chamber inlet and this is compared with the calibration obtained in the laboratory and

determined in flight by an array of monitors. The in-flight calibration system consists of two Hg lamps, filtered to pass only 185 nm, and photodiode detectors to monitor the Hg lamp flux. These are placed in the inner nacelle wall, just upstream of the sampling inlet. The 185 nm radiation photolyzes ambient water vapor to produce OH + H, and the H atom readily reacts with O_2 to produce an amount of HO_2 equal to that of OH. The initial velocity field is calculated (K. James, personal communication), and are being tested.

An ATHOS electronics block diagram is shown in Figure 2. The PSMCU is the power supply and motor control unit; the DAU is the data acquisition unit. The DOS computer uses Lab Windows graphing and menu routines. Sampling occurs 5 times a second. The instrument operation uses an ASCII configuration file to set instrument operation. Many instrument functions are automated; a manual override allows for operator intervention. Both text and strip charts are used to display data during the flight.

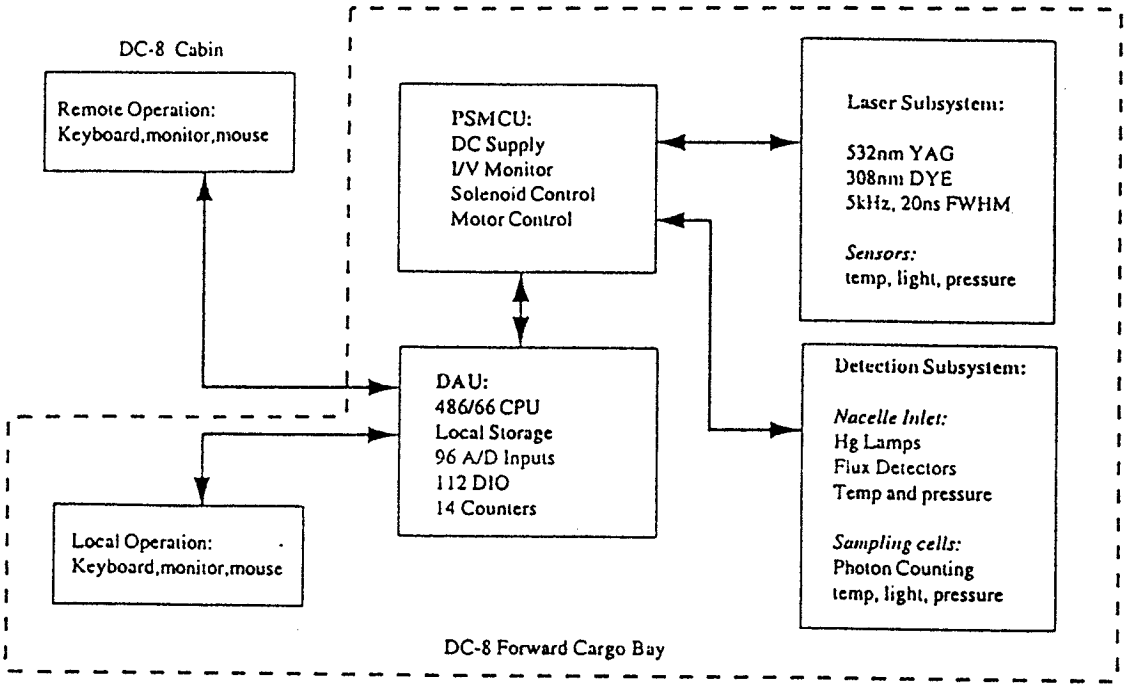

Figure 2. Block diagram of the ATHOS Electrical System.

Preliminary Results from SUCCESS.

SUCCESS was designed to study the radiation and microphysics associated with cirrus clouds and contrails. The upload for this mission began in late February and the mission itself, mostly based in Salina, Kansas, occurred from 13 April to 15 May. ATHOS was put on the DC-8 for SUCCESS so that it could have some engineering test flights. The hope was that in the process some good OH and HO_2 measurements could be made. ATHOS measured OH measurements for all or part of all 19 flights, and HO_2 for all or part of 9 flights. Data quality improved substantially over the course of SUCCESS as thermal stability was improved and more in-flight test procedures were developed. High-quality OH and HO_2 measurements will be available to the scientific community for most of SUCCESS once post-flight calibrations and tests are complete.

A number of questions can be answered about the performance of ATHOS during SUCCESS. These are based on a preliminary look at the data, which is now being processed in greater detail.

What is the sensitivity of ATHOS?

The sensitivity of ATHOS has been determined by a combination of laboratory calibrations and in-flight monitors. For the SUCCESS archive data, we average 100 seconds of data, 50 seconds on-line and 50 seconds off-line, or 5 cycles. We find the OH mixing ratios by the equation:

$$\chi_{OH} = (\text{Signal}_{\text{on-line}} - \text{Signal}_{\text{off-line}}) / (C),$$

where C is determined by laboratory calibrations that are corroborated by in-flight calibrations and laser power and laser-scattering monitors. The minimum detectable [OH] we define as the OH derived from twice the standard deviation of the background signal:

$$[OH]_{min} = 2\ (2 \times \text{background signal})^{1/2} / \{C_{[OH]} \times (\text{time})^{1/2}\}$$

where $C_{[OH]} = C / [M]$.

Using these equations, the laboratory calibrations, and data from 10 May 1997, we get the preliminary information in Table 2. We use the mixing ratio units ppqv = 10^{-15}. [OH] for this flight was typically (1.5-3)x10^6 cm^{-3}, while $[OH]_{min}$ was (2.1-3.5)x10^5 cm^{-3}. The last column, σ_{OH}, is the variation of several 100-second OH values for the altitudes and time periods around and including those of the raw data shown. The simultaneous variation of NO at 12, 9.5, and 7 km was about 30%, 100%, and <20% peak-to-peak for the same time periods. Thus, σ_{OH} is more than twice $[OH]_{min}$ because of the NO variations. The small σ_{OH} at 7 km indicates the instrument measurement variability. The present absolute uncertainty, determined from a combination of laboratory calibrations and instrument monitors, is about ±50%, at the 2 sigma uncertainty limit.

Alt (km)	ΔS (cts/s)	C (cts/s)	χ_{OH} (ppqv)	[M] (cm^{-3})	[OH] (cm^{-3})	$C_{[OH]}$ (cts/s)/cm^{-3}	$[OH]_{min}$ (cm^{-3})	$\sigma_{[OH]}$ (cm^{-3})
12.0	12.7	$5.3x10^{13}$	240	$6.8x10^{18}$	$1.6x10^{6}$	$7.8x10^{-6}$	$2.1x10^{5}$	$1.9x10^{5}$
							= 31 ppqv	= 28 ppqv
9.5	14.2	$4.4x10^{13}$	320	$9.0x10^{18}$	$2.9x10^{6}$	$4.9x10^{-6}$	$3.5x10^{5}$	$5.0x10^{5}$
							= 39 ppqv	= 56 ppqv
7.0	9.7	$6.4x10^{13}$	150	$1.17x10^{19}$	$1.8x10^{6}$	$5.5x10^{-6}$	$3.2x10^{5}$	$1.2x10^{5}$
							= 27 ppqv	= 10 ppqv

Table 2. Signals, calibrations, mixing ratios, and variability from 10 May 1996 during SUCCESS (100-second averages)

These data show that ATHOS easily detects ambient OH with a S/N ratio of 10 in 100 seconds. The instrument operation on this flight was fairly typical; both slightly better and slightly worse sensitivity occurs on other flights.

An example of OH signals is shown in Figure 3, data from 27 April, 1996.

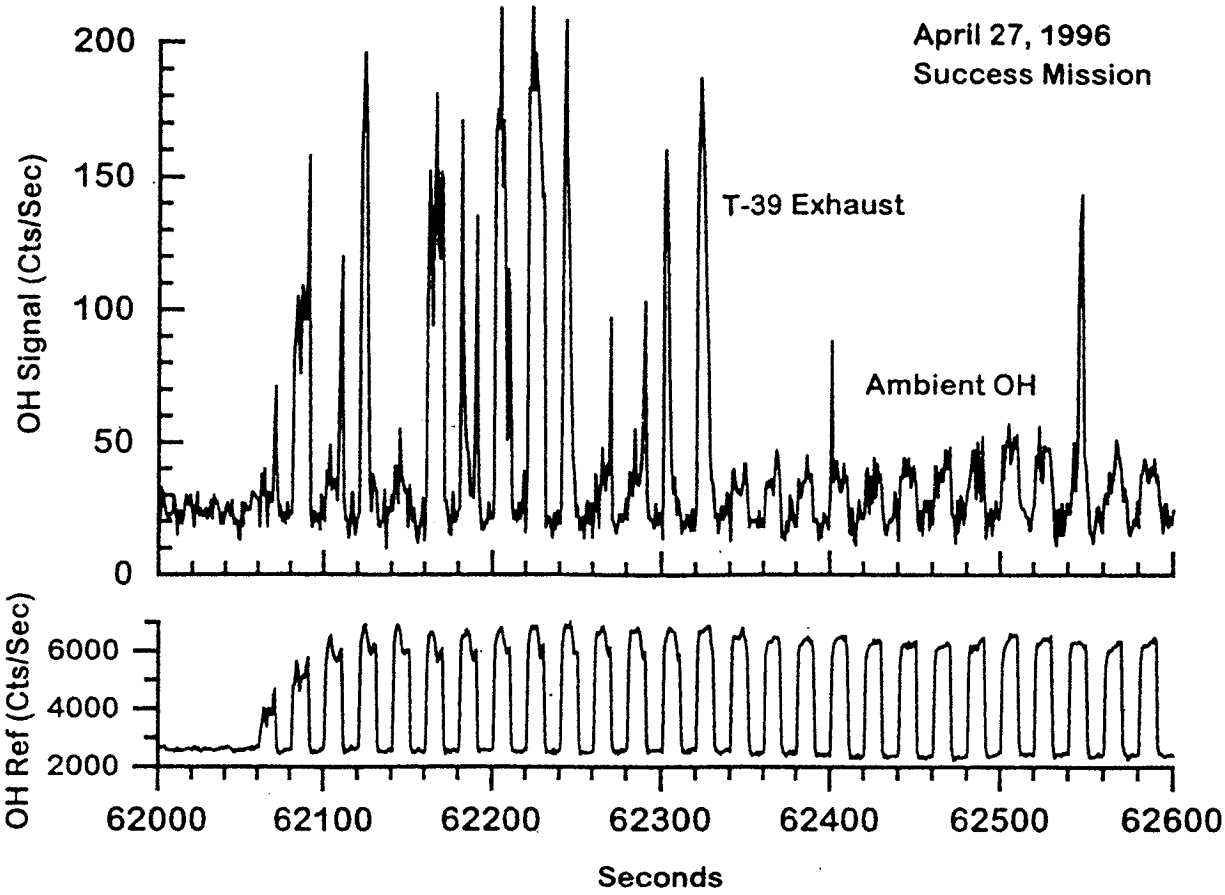

Figure 3. OH Signals from 27 April, 1996.

The high OH reference signal indicates when the laser wavelength is tuned to the OH resonance and is detecting OH. A comparable waveform is seen in the raw OH signal as well. The large OH signals occur in the T-39 exhaust. The raw 5-Hz data have been summed into 1 second binds for this display, but statistically significant signals are possible even at 5 Hz. The period between 62000 and 62060 seconds shows the variation in the background signal because the laser was kept off-line. The period between 62400 and 62540 is a measurement of ambient OH for this altitude of 11 km.

As the laser beam passes down to the OH detection axes, a beam-splitter diverts about 10% of the light to the HO_2 detection axis. However, because about 40-50% of the OH is lost on the sampling tube wall between the inlet and the detection cell while <10% of the HO_2 is lost, according to laboratory calibrations, the relative sensitivity of the OH and HO_2 detection axes is a factor of 6, not a factor of 9 that was measured for the OH detection sensitivities of the two axes. The conversion efficiency for the reaction of NO with HO_2 to make OH is better than 95%. This conversion was checked frequently in the laboratory and in-flight using the Hg lamp as a source of equal amounts of OH and HO_2. The limit of detection for HO_2 was about $6x10^5$ molecules cm^{-3} for S/N=2 and 100 seconds total integration time.

Does the nacelle assembly slow the air flow without perturbations?

For the flights that have been examined in detail, the nacelle assembly appears to work. A thermistor array consisting of 7 thermistors spans the inside of the inner nacelle 3 cm behind the inlet. It shows no intrusion of boundary layer air into the nacelle (all thermistors read the same temperature). The pitot tube is located inside the inner nacelle in a position that is the same distance from the wall and from the front of the nacelle as the sampling inlet, but is rotated 160 degrees toward the bottom of the nacelle. The range of air speeds measured is 7 to 40 m s^{-1}, slightly faster than the target velocity range of 5 to 30 m s^{-1}. The flow is well-behaved, and shows no perturbations. These indicators and OH measurements give strong evidence that the nacelle assembly is working.

We did have difficulty moving the centerbody, which controls the air speed at the inlet, because the motor that moves the front on the centerbody was underpowered. However, we were able to move the centerbody backwards and then occasionally forwards if the aircraft was slowed briefly. The variation in the air speed in the inner nacelle is an important diagnostic of the airflow and of the in-flight calibration system.

What are the inlet and wall losses in ATHOS?

Evidence suggests that inlet losses of OH and HO_2 are small for ATHOS. First, the OH and HO_2 signals did not change significantly as the aircraft underwent MMS pitch and yaw maneuvers for the MMS calibration. An example is shown in Figure 4. Second, the OH signal changes less than 10% as the velocity at the sampling inlet is increased from 8 m s^{-1}

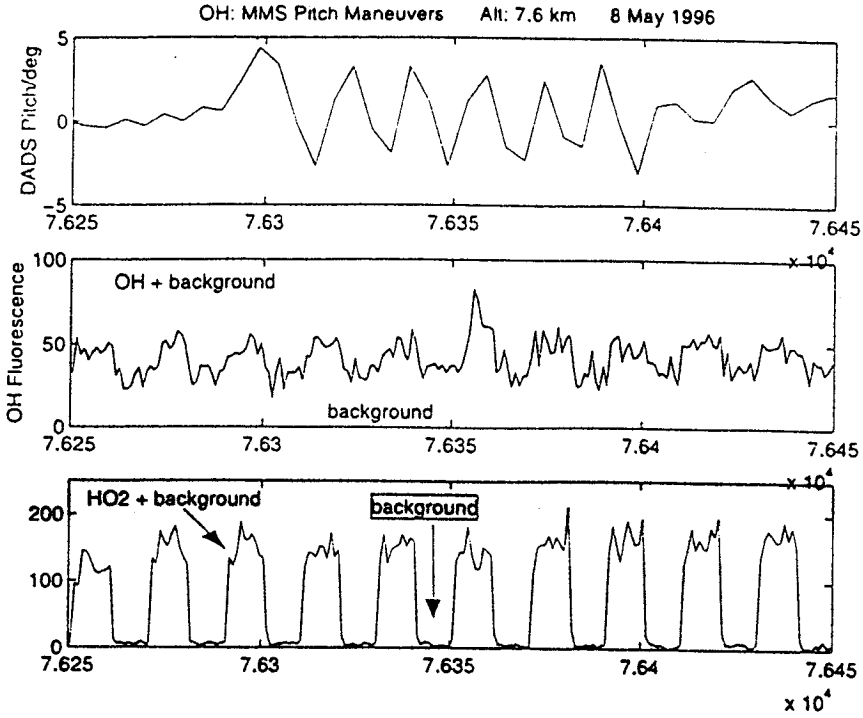

Figure 4. Variation of OH and HO_2 signals during MMS pitch maneuvers, 8 May 1996. The DC-8 pitch goes from +4° to -3°. No change can be seen in either the OH or the HO_2 signals. The 2-second rise in OH near 763505 seconds appears to correspond to a dip in HO_2 and does not appear on the other MMS pitch cycles.

to 38 m s^{-1}. In addition, the excellent agreement between the FAGE-type instrument and the multiply-folded long path absorption instrument from Juelich during the POPCORN campaign indicates that any inlet loss for the Juelich FAGE-type instrument is the same during calibrations and measurement. Our detection hardware is very similar to theirs. We have tried many different inlet designs and materials. We have found that bad designs reduce the OH signal, but good designs all give the same OH signal. Thus, while we continue to pursue this issue, we have never had any evidence for OH inlet loss.

The need to sample air outside of the aircraft boundary layer results in the 39-cm long sampling tube. Laboratory studies show that sampling tube lengths of as much as 15 cm can be used without any indication of OH loss. Laboratory studies have shown that 50-60% of the OH outside the sampling inlet is detected at the OH axis for a 39 cm long tube; 45-50% is detected at the HO_2 axis 10 cm downstream from the OH axis. These studies also show that >90% of the HO_2 is detected at the HO_2 axis. The OH losses are consistent with the calculated residence time in a cylinder if we assume that OH is lost on every collision. The sensitivity ratio has been checked both in the laboratory and during the in-flight calibrations for the SUCCESS flights.

ATHOS with the current vacuum system is not wall-less. The two main concerns are that the wall loss is not constant and that OH and HO_2 are created on the walls under certain circumstances. The fact that the HO_2/OH ratio is constant over a number of flights suggests that the wall loss is not changing. The wall-loss constancy will be tested in a series of post-flight calibrations. Laboratory studies both pre- and post-flight have shown that no OH or HO_2 signals are observed when ambient OH and HO_2 are zero. Pre-flight tests in the early morning of 10 May 1996 during SONEX also indicate that no OH is being created within the instrument. While these studies provide evidence that the walls are having no effect on the OH and HO_2 measurements, this issue will continue to be further tested.

Do interfering signals contaminate the OH and HO_2 signals?

All evidence suggests that no interfering signals are contaminating the OH and HO_2 signals. First, laser-generated OH has not been observed either in the laboratory or in a nighttime preflight check prior to the 10 May 1996 flight during SUCCESS. During that test, the off-line signal was statistically the same as the on-line signal, so that the upper limit to interfering OH is less than 5×10^4 molecules cm^{-3}. In addition, laser-generated OH should be proportional to the square of the OH laser power. However, the observed OH is linearly proportional to laser power (Figure 5), indicating no laser-generated OH. These observations are not surprising. We have never seen any laser-generated OH with 308 excitation, as expected from calculations.

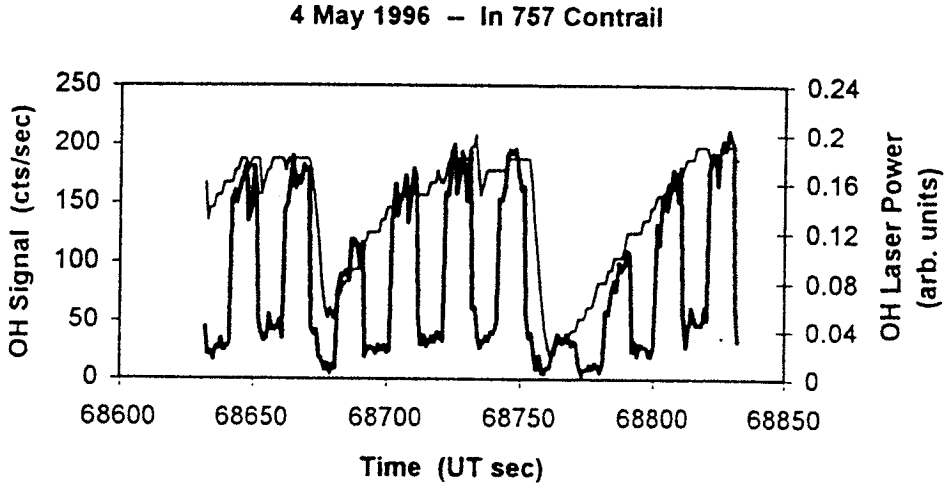

Figure 5. Variation of OH signal and laser power in the 757 contrail, 4 May 1996. The heavy line is the OH signal, where the large signals are on-line and the small ones off-line. The light line is the laser power exiting the OH White cell. Laser instabilities cause the sudden changes in laser power. Note the excellent correspondence between the laser power and the OH signal. Other occasions show that the OH and HO_2 signals are constant when the DC-8 remained in the 757's exhaust as it did here.

Second, previous ground-based studies show no evidence of interfering signals (Stevens et al., 1994), even under highly polluted conditions. Even the background signal remains unaffected. Note the constancy of the background signals in Figure 3 even as the DC-8 goes in and out of the T-39 exhaust. A good test of interfering signals is nighttime measurements. A sunrise flight, with more than an hour in darkness, was planned for 10 May 1996. However, a sudden and furious thunderstorm delayed the flight until after sunrise. We will attempt this test on future missions.

Are there any "non-statistical" background signals, as have been suggested by earlier attempts at OH measurements?

We have examined a few SUCCESS flights in some detail. In clear air, the standard deviations of the means for the OH and HO_2 off-line background signals are as expected from Poisson counting statistics when the laser fluctuations are first removed. For the typical off-line background signals of 25 cts s^{-1}, the standard deviation of the mean is 5±1 cts s^{-1}. Further, the background signal varies little with wavelength, indicating that no unusual species contribute to a spectrally dependent scattering. Thus, we do not observe the "non-statistical" background signal discussed by Bradshaw et al. (1984). As a result, the limit of detection and the S/N ratio improve with the square root of time.

Over what altitude range can ATHOS measure OH and HO_2?

SUCCESS flights tended to remain at high altitudes in order to sample cirrus clouds and contrails. An altitude profile for OH is shown in Figure 6 for the 29 April 1996 flight. Each data point is a 100-second average. Much of the OH variability is due to variations in NO, O_3, and CO.

Another example of a descent is shown in Figure 7. The aircraft was descending from 12 km down to 4 km on 10 May 1996 during SUCCESS. Both OH and HO_2 were measured on this flight. The aircraft was flown in a descending stair-step pattern in a race track over California. OH and HO_2 at 220 hPa (about 12 km) increase with sunrise during the transit from Kansas to California, where the descent was made. Data from this flight and others show that the OH mixing ratio is typically 0.1 to 1 pptv, while the HO_2 mixing ratio is typically 2 to 20 pptv. When compared to computer models, both simple steady-state models and more complex models, the measured OH and HO_2 mixing ratios tend to be equal to or larger than the modeled OH and HO_2 mixing ratios, while the observed HO_2/OH ratio is roughly equal to modeled HO_2/OH ratio. Differences did occur, and these are subject of ongoing study.

Can ATHOS measure OH and HO_2 in clouds?

SUCCESS provided many opportunities to test the ability of ATHOS to measure OH and HO_2 in and around clouds. Thin clouds did not effect either the on-line or the off-line signal quality. Denser clouds do affect the background signal. However, the OH signal can be recovered even above the changing background because the Rayleigh scattering

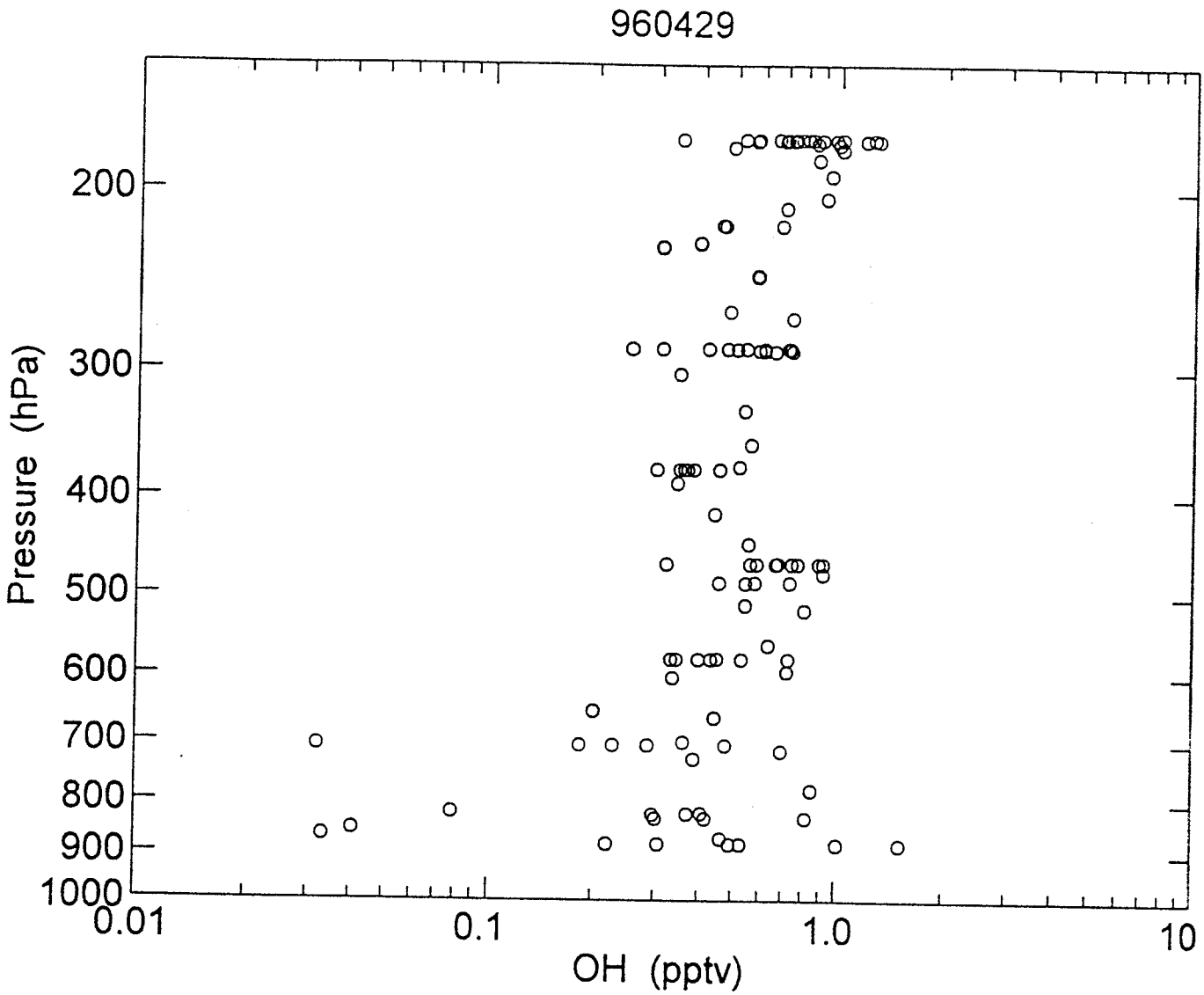

Figure 6. Altitude profile of the OH mixing ratio over Oklahoma, 29 April 1996. the approximate altitude range is 2 km to 12 km. Much of the flight was in clouds, which may be the cause of some of the observed scatter in the observations.

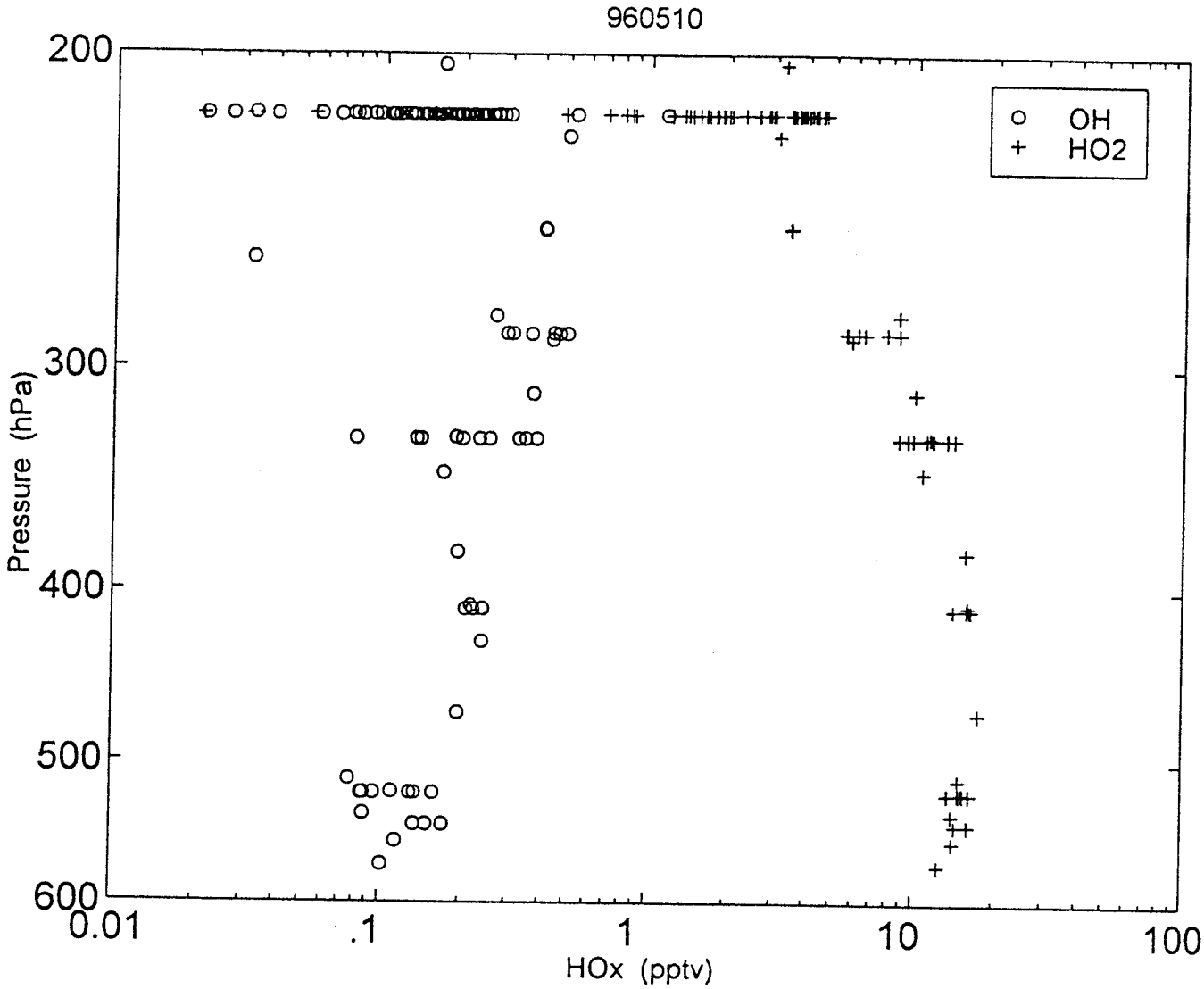

Figure 7. Altitude profiles of OH and HO_2 mixing ratios observed over California, 10 May 1996.

An example of this process is shown in Figure 8 in a cirrus cloud on 15 May 1996. The 4 signals are the raw 1-Hz OH signal, the Rayleigh scattering signal, the OH reference signal. which indicates when the laser wavelength is on-line (high) and off-line (low), and the OH difference signal (shifted by -80 cts s^{-1} on the plot and smoothed with a 3-point running average). The OH difference signal is found by relating the OH fluorescence background signal to the Rayleigh signal, using this relationship to determine the background signal, even underneath the OH fluorescence signal, and then subtracting this derived background signal from the OH signal. The resulting OH difference signal shows the square-wave profile with a 15 cts s^{-1} amplitude that mimics the OH reference signal. Closer examination reveals that the background subtraction applied here is not perfect and can be improved. The clear air Rayleigh signal was 1900 cts s^{-1}. Thus, the measurement was in the cloud from roughly 72280 s to 72410 s. OH appears to decrease in the cloud. HO_2, which is less effected by increases in the background signal, shows about a 25% decrease at the same time. A more complete analysis using particle and other chemical data will determine what this result means.

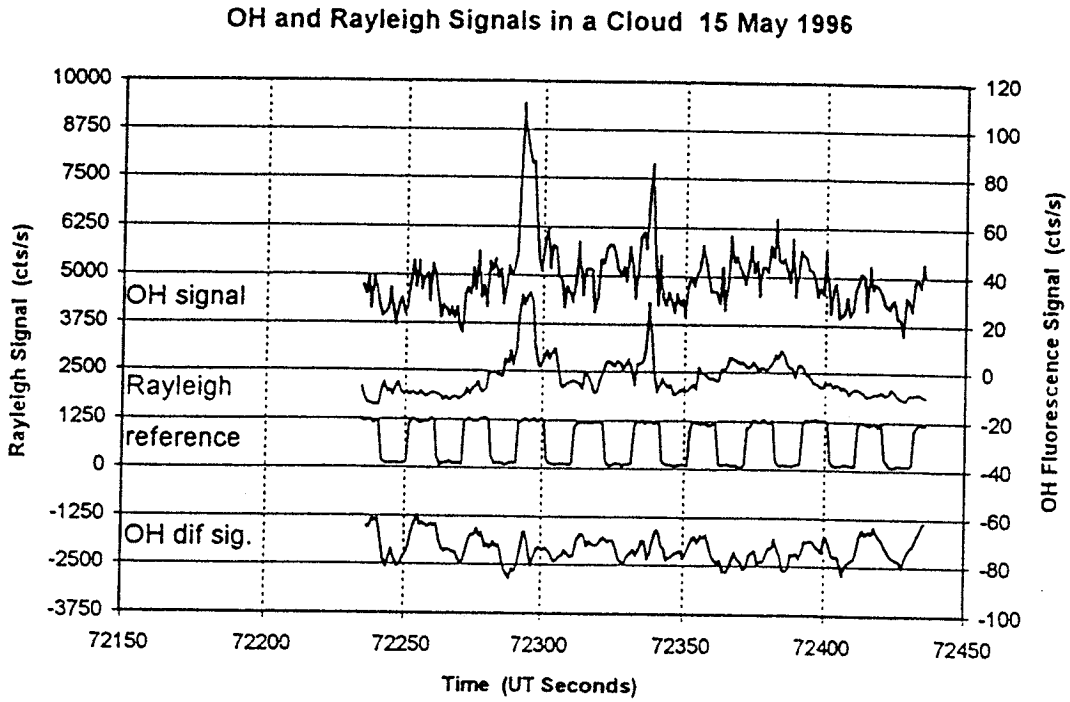

Figure 8. OH measurements in a cloud, 15 May 1996. Top curve is the raw, 1-Hz OH signal (right scale); second curve is the Rayleigh scattering of the OH detector (left scale); third curve is the OH reference cell signal (on-line and off-line) (left scale); last curve is the OH difference signal with the background corrected by the Rayleigh scattering signal (right scale; scale shifted so that -80 = 0 cts/s).

Summary.

NASA-Ames Grant No. NAG 2-938, "Adaption of an in situ ground-based tropospheric OH/HO_2 instrument for aircraft use" is successfully completed. The resulting instrument, ATHOS, is now available for measurements of OH and HO_2 during missions of the NASA DC-8.

The instrument performance was greatly improved during the 19 flights of SUCCESS. In-flight and laboratory diagnostics show that ATHOS is sensitive enough for measurements of atmospheric OH and HO_2, apparently free from interferences, and capable of measuring OH and HO_2 over the entire troposphere and lower stratosphere, as well as in thin clouds and contrail exhaust. The observations from SUCCESS are yielding a wealth of new information about atmospheric OH and HO_2.

References

Ashmutat, U., M. Hessling, F. Holland, and A. Hofzumahaus, A tunable source of hydroxyl (OH) and hydroperoxyl (HO_2) radicals: In the range between 10^6 and 10^9 cm^{-3}, in *Physico-Chemical Behavior of Atmospheric Pollutants*, edited by G. Angeletti and G. Restelli, 811-816, European Commission, Brussels, 1994.

Bradshaw, J. D., M. O. Rogers, and D. D. Davis, 1984: Sequential two-photon laser-induced fluorescence: A new technique for detecting hydroxyl radicals, *Appl. Opt., 23*, 2134.

Brune, William, H., Philip S. Stevens, and James H. Mather, 1995: Measuring OH and HO_2 in the troposphere by laser-induced fluorescence at low pressure, *J. Atmos. Sci, 52*, 3328-3336.

Crosley, D.R., 1993a: Local measurements of tropospheric HO_x, *SRI International Report MP 92-135*, SRI International, Menlo Park CA.

Crosley, David R., 1995: The measurement of OH and HO_2 in the atmosphere. *J. Atmos. Sci, 52*, 3299-3314.

Eisele, F.L., and D.J. Tanner, 1991: Ion-assisted tropospheric OH measurements, *J. Geophys. Res., 96*, 9295.

Eisele, F.L., 1995: New insight and questions resulting from recent ion-assisted OH measurements, *J. Atmos. Sci, 52*, 3337-3341.

Hard, T.M., R.J. O'Brien, C.Y. Chan and A.A. Mehrabzadeh, 1984: Tropospheric free radical determination by FAGE, *Environ. Sci. Technol., 18*, 768.

Hard, T. M., A. A. Mehrabzadeh, C. Y. Chan, and R. J. O'Brien, 1992: FAGE measurements of tropospheric HO with measurements and model of interferences, *J. Geophys. Res., 97*, 9795.

Hard, T.M., L.A. George, and R.J. O'Brien, 1995: FAGE Determination of Tropospheric HO and HO_2, *J. Atmos. Sci, 52*, 3354-3372.

Mather, J.H., et al., OH and HO_2 measurements using laser-induced fluorescence, *J. Geophys. Res., 102*, 6427-6436, 1997.

O'Brien, R.J., and T.M. Hard, 1993: Tropospheric hydroxyl radical: a challenging analyte, *Adv. Chem. Ser. 232*, 323.

Stevens, P.S., J.H. Mather, and W.H. Brune, 1994: Measurement of tropospheric OH and HO_2 by laser-induced fluorescence at low pressure, *J. Geophys. Res., 99*, 3543-3557.

Thompson, Anne M., 1995: Measuring and modeling the tropospheric hydroxyl radical (OH). *J. Atmos. Sci, 52*, 3315-3327.

Wennberg, P.O., et al., 1994: Aircraft-borne, laser-induced fluorescence instrument for the in situ detection of hydroxyl and hydroperoxyl radicals, *Rev. Sci. Instrum., 65*, 1858.

Wennberg, P.O., T.F. Hanisco, R.C. Cohen, R.M. Stimpfle, 1995: In situ measurements of OH and HO_2 in the upper troposphere and stratosphere, *J. Atmos. Sci, 52*, 3413.